Author Manuscript

Author Manuscript

Author Manuscript

Author Manuscript

HHS Public Access

Author manuscript

Acta Biomater. Author manuscript; available in PMC 2016 September 20.

Published in final edited form as:

Acta Biomater. 2016 March ; 33: 25–33. doi:10.1016/j.actbio.2016.02.004.

Increasing the strength and bioactivity of collagen scaffolds using customizable arrays of 3D-printed polymer fibers

Laura C. Mozdzen[a], **Ryan Rodgers**[a], **Jessica M. Banks**[b], **Ryan C. Bailey**[b], and **Brendan A.C. Harley**[a,c,*]

[a]Department of Chemical and Biomolecular Engineering, University of Illinois at Urbana-Champaign, Urbana, IL 61801, United States

[b]Department of Chemistry, University of Illinois at Urbana-Champaign, Urbana, IL 61801, United States

[c]Carl R. Woese Institute for Genomic Biology, University of Illinois at Urbana-Champaign, Urbana, IL 61801, United States

Abstract

Tendon is a highly aligned connective tissue which transmits force from muscle to bone. Each year, people in the US sustain more than 32 million tendon injuries. To mitigate poor functional outcomes due to scar formation, current surgical techniques rely heavily on autografts. Biomaterial platforms and tissue engineering methods offer an alternative approach to address these injuries. Scaffolds incorporating aligned structural features can promote expansion of adult tenocytes and mesenchymal stem cells capable of tenogenic differentiation. However, appropriate balance between scaffold bioactivity and mechanical strength of these constructs remains challenging. The high porosity required to facilitate cell infiltration, nutrient and oxygen biotransport within three-dimensional constructs typically results in insufficient biomechanical strength. Here we describe the use of three-dimensional printing techniques to create customizable arrays of acrylonitrile butadiene styrene (ABS) fibers that can be incorporated into a collagen scaffold under development for tendon repair. Notably, mechanical performance of scaffold-fiber composites (elastic modulus, peak stress, strain at peak stress, and toughness) can be selectively manipulated by varying fiber-reinforcement geometry without affecting the native bioactivity of the collagen scaffold. Further, we report an approach to functionalize ABS fibers with activity-inducing growth factors via sequential oxygen plasma and carbodiimide crosslinking treatments. Together, we report an adaptable approach to control both mechanical strength and presence of biomolecular cues in a manner orthogonal to the architecture of the collagen scaffold itself.

Graphical Abstract

*Corresponding author at: Department of Chemical and Biomolecular Engineering, Carl R. Woese Institute for Genomic Biology, University of Illinois at Urbana-Champaign, 110 Roger Adams Laboratory, 600 S. Mathews Ave., Urbana, IL 61801, United States. bharley@illinois.edu (B.A.C. Harley).

Appendix A. Supplementary data

Supplementary data associated with this article can be found, in the online version, at http://dx.doi.org/10.1016/j.actbio.2016.02.004.

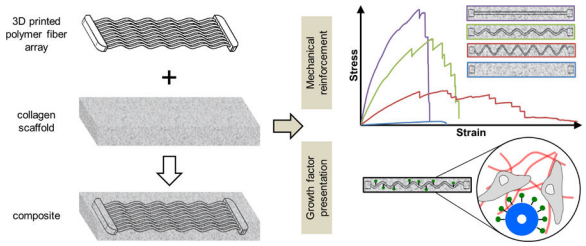

Keywords

Composite CG scaffolds; Tunable mechanics; Tendon tissue engineering; Three-dimensional printing

1. Introduction

Tendons are highly aligned tissues made from a hierarchical alignment of type I collagen fibrils which transmit force from muscle to bone. Each year, chronic and acute tendon injuries account for more than 32 million injuries in the US alone [1]. Healing of these injuries can be complicated by the scale of the defect, the age and physical activity of the patient, as well as resultant inflammatory response post-injury. While relatively minor tendon injuries may heal on their own, major tendon injuries result in scar formation which hinders mechanical performance and often results in pain and poor functionality. Current surgical techniques rely heavily on autografts and allografts [2]. Although these techniques are successful for some, they become problematic for recurrent injuries. Biomaterials for tissue engineering are becoming a popular approach to address these injuries and have a significant potential to replace allografts and autografts for many classes of complex tendon and ligament injuries. However, significant hurdles, particularly mechanical optimization, remain [3].

Collagen-glycosaminoglycan (CG) scaffolds belong to a versatile class of porous biomaterials that have been used for a wide range of tissue engineering applications. Fabricated via lyophilization from a suspension of extracellular matrix (ECM) derived proteins, these scaffolds present a porous network (typically greater than 95% porous) that supports cell invasion and metabolite biotransport [4,5]. Here, individual pores of order 50–250 μm in size are defined by fibers of collagen content, termed struts, which provide alignment, compositional, and stiffness cues to cells within the network. Originally developed to promote scarless healing in dermis [6,7] and peripheral nerves [8], the ability to precisely control microstructural features (pore size, shape) of these scaffolds has been exploited to examine mechanistic details regarding how scaffold biophysical properties affect cell adhesion, migration, and contraction [4,6,9,10]. More recently, variants of these scaffolds have been developed towards the promotion of healing a wider range of tissues including tendon [11–13], bone [14–16], cartilage [14,17,18], and orthopedic insertions (tendon-bone; cartilage-bone) [19,20].

Emerging efforts have focused on developing strategies that use the scaffold to provide instructive signals that selectively promote a desired cell behavior such as proliferation,

Author Manuscript Author Manuscript Author Manuscript Author Manuscript

Author Manuscript Author Manuscript Author Manuscript Author Manuscript

migration, or functional phenotype. Mineral content and bioactive glass can be included into the scaffold to enhance mesenchymal stem cell (MSC) osteogenic differentiation and bone repair [19,21–23]. Similarly, aligned networks of ellipsoidal pores generated via directional solidification have been exploited for applications in anisotropic tissue engineering (*e.g.*, cardiac, tendon) [24]. Biomolecular signals are particularly popular, and multiple strategies have been explored to incorporate growth factors within these collagen scaffolds. We and others have described the optimization of individual factors or combinations of soluble growth factors in the context of musculoskeletal repair [25–27]. In order to combat diffusive loss of these factors, additional efforts have described modifications to promote ubiquitous or spatially-patterned covalent immobilization of growth factors within the scaffold network [28–31]. More recently, we have also described the use of scaffold proteoglycan chemistry to promote transient sequestration of growth factors within the CG scaffold via non-covalent interactions [32,33].

Efforts in our lab have recently focused on the development of a new class of scaffold for regenerative repair of orthopedic insertions, notably the osteotendinous (tendon-bone) junction [19]. While CG scaffolds display advantageous bioactive characteristics particularly in the realm of promoting cell expansion and metabolic health, one particular disadvantage which has yet to be adequately addressed is the sub-optimal mechanical strength. Healthy tendon, trabecular bone, and the osteotendinous insertion each have elastic moduli well in excess of 10 MPa [34–38]. CG scaffolds typically exhibit porosities in excess of 95% (relative density: <5%) in order to provide sufficient specific surface area for initial cell attachment as well as to facilitate nutrient biotransport [4,39]. However, this high porosity leads to low mechanical strength, with typical elastic moduli of order 20–200 kPa (dry) and 1–50 kPa (hydrated) [19,40,41]. While this stiffness can be increased through the selective addition of mineral content or crosslinking, the native stiffness of these scaffolds is still more than two orders of magnitude too soft [40]. Although tissue engineering constructs do not need to exactly match the tissue they are implanted into, they do need to withstand daily *in vivo* mechanical forces without permanently deforming or failing. And while increasing the relative density of the scaffold leads to significant increases in the macroscopic scaffold modulus [40,42], such increases come at a cost of reduced cell penetration and metabolic health. And while cellular remodeling can lead to significant increases in the mechanical strength of the construct, the timescale for remodeling makes it impractical to rely on it as an initial stiffening strategy [43].

Bioinspired designs offer an alternative paradigm for addressing current trade-offs between scaffold modulus and biotransport-influenced bioactivity. Inspired by core–shell composite structures such as those found in the porcupine quills and plant stems [44,45], we recently described the integration of a high-density collagen membrane *shell* to the porous (low-density) collagen scaffold *core* capable of increasing the overall construct elastic modulus by over 30-fold [13]. We added periodic perforations to the shell to improve biotransport and cell penetration into the scaffold [46]. While effective, the shell limited the capacity to rapidly produce constructs of arbitrary shape to address many osteotendinous injuries. So here we describe efforts to create a different reinforced scaffold composite inspired by the longitudinal fibers found as reinforcing structures in plant stems. This effort is enabled by the recent rapid proliferation of commercial three-dimensional printing tools. Here we report

Author Manuscript Author Manuscript Author Manuscript Author Manuscript

a prototype scaffold-fiber composite fabricated from a CG scaffold impregnated with arrays of acrylonitrile butadiene styrene (ABS) fibers generated using a commercial three-dimensional printing platform. This effort looks to combine the poor mechanical strength yet high biocompatibility of the CG scaffold with the superior mechanical properties but poor biocompatibility of ABS in a single composite. We explore the use of different fiber morphologies as a means to customize the composite mechanical behavior, as well as approaches to functionalize the fiber reinforcement array with biomolecules to enhance cellular bioactivity.

2. Materials and methods

2.1. Preparation of collagen-GAG precursor suspension

A CG suspension was prepared from type I collagen (1.0% w/v) isolated from bovine Achilles tendon and chondroitin sulfate (0.1% w/v) derived from shark cartilage in 0.05 M acetic acid (Sigma–Aldrich, St. Louis, MO). The suspension was homogenized at 4 °C to prevent gelatinization during mixing and was degassed before use [47].

2.2. Fabrication of acrylonitrile butadiene styrene fiber arrays via 3D printing

A series of acrylonitrile butadiene styrene (ABS) fiber arrays were created then incorporated into CG scaffolds to evaluate the effect of ABS fiber reinforcement on scaffold mechanical properties. Each array consisted of 9 parallel 1 mm diameter ABS fibers fixed together at either end with ABS end blocks (end blocks: 20 × 4 × 3 mm; complete fiber array: 20 × 76 × 3 mm) (Fig. 1). Three different fiber geometries of theoretically decreasing elastic modulus were fabricated: a parallel array of 9 linear fibers (*straight fiber array*); a parallel array of 9 sinusoidal fibers with 1 mm amplitude (period: 11.3 mm; *1 mm sinusoidal fiber array*); a parallel array of 9 sinusoidal fibers with 2 mm amplitude (period: 11.3 mm; *2 mm sinusoidal fiber array*). Alternatively, ABS end blocks not connected by fibers were used as a negative control (*scaffold alone*). All constructs were printed using a MakerBot Replicator 2× (MakerBot Industries, Brooklyn, NY) at standard quality settings (10% infill, 2 shells, 200 μm layered height) and an extruder speed of 90 mm/s. To ensure structural fidelity of the fiber arrays, ABS fibers were co-printed with polystyrene supports using dual nozzles (polystyrene: 250 °C; ABS: 230 °C) onto a temperature controlled build-plate (110 °C). The polystyrene supports were subsequently dissolved in D-Limonene (GreenTerpene, Miami, FL), leaving behind the final ABS fiber array. After all polystyrene was dissolved, ABS fiber arrays were washed multiple times with deionized water, and then dried before use.

2.3. Fabrication of ABS fiber reinforced CG scaffolds via lyophilization

ABS fiber arrays or ABS end blocks alone were placed into aluminum molds 7.6 cm (long) × 2 cm (wide). The CG suspension was then added to submerge the fiber array, with the final ABS–CG composite fabricated via a previously described lyophilization protocol [48]. Briefly, the mold was placed on a freeze-dryer shelf (VirTis, Gardiner, NY) maintained initially at 20 °C. The shelf temperature was then ramped down to −40 °C at a rate of 1 °C/min, followed by a 1 h hold at −40 °C to ensure complete solidification. Following freezing, the shelf temperature was ramped up to 0 °C at a rate of 1 °C/min, after which a 200 mTorr vacuum was maintained overnight to remove ice crystals via sublimation [40,48], leaving

Author Manuscript Author Manuscript Author Manuscript Author Manuscript

behind the porous CG scaffold impregnated with ABS fibers (Fig. 1A). The CG–ABS fiber-reinforced scaffolds were dehydrothermally crosslinked at 105 °C for 24 h under vacuum (<25 torr) in a vacuum oven (Welch, Niles, IL) [49]. After DHT crosslinking, scaffolds were stored under desiccation until use.

2.4. SEM analysis of fiber-scaffold composite microstructure

In order to visualize the degree of penetration of the CG scaffold into the ABS fiber array, transverse sections were cut through the CG–ABS composites with a razor blade in order to expose the interior structure of the composites. Transverse sections were subsequently imaged with scanning electron microscopy (SEM) on a JEOL JSM-6060LV (JEOL USA) to assess both the degree of CG scaffold penetration within the ABS fiber array as well as the presence of any voids between the ABS surface and the surrounding CG scaffold. A combination of secondary and backscatter electron detection were used under low vacuum to image the CG–ABS fiber array composite.

2.5. Tensile testing of ABS–CG composites

The elastic modulus of CG–ABS fiber array composites (7.6 cm × 2 cm× 5 mm thick) were assessed via uniaxial tension tests. Tensile mechanical tests were performed on dry scaffold fiber composite samples (5 cm gauge length) at a rate of 5.0 mm/min using an MTS Insight electromechanical load frame (Eden Prairie, MN), with tensile grips gripping the ABS end blocks embedded within each scaffold. Tests were performed on scaffolds ($n = 6/-$ group) containing: end blocks only (no connecting fibers; *scaffold alone*); a parallel array of 9 sinusoidal fibers with 2 mm amplitude (*2 mm sinusoidal fiber array*); a parallel array of 9 sinusoidal fibers with 1 mm amplitude (*1 mm sinusoidal fiber array*); a parallel array of 9 linear fibers (*straight fiber array*). The elastic modulus of each construct was calculated by taking the slope of the linear region (0.5–5% strain) of the stress–strain curve for each sample. Construct toughness was calculated analytically from the area under the stress–strain curve for each sample. Additionally, for each test overall peak stress (maximum load divided by sample cross-sectional area) and strain at peak stress were also calculated.

2.6. Functionalizing ABS constructs with biomolecules

In order to immobilize a biomolecule of interest to ABS constructs, the constructs were cleaned via oxygen plasma (no gas flow, high RF,<0.3 torr, 5 min per side; PDC-32G, Harrick Plasma, Ithaca, NY) in order to expose carboxylic acid groups on the ABS surface (Supplemental Fig. 1). Fibers were subsequently functionalized with either a model protein, bovine serum albumin (BSA), or platelet derived growth factor BB (PDGF-BB), known to enhance cell metabolic activity in CG scaffolds [26]. Plasma-cleaned ABS constructs were incubated with BSA (100 μg/mL) or PDGF (1 μg/mL) [50] in the presence of a solution of 1-ethyl-3-[3-dimethylaminopropyl] carbodiimide hydrochloride (EDC) and N–hydroxysulfosuccinimide (NHS) (5 mg/mL, 1 h) to catalyze the formation of covalent crosslinks between the plasma cleaned ABS and the biomolecule of interest. Samples were washed in PBS and stored for future use. To quantify the degree of biomolecular attachment, fluorescently labeled BSA (BSA-Alexafluor-594 conjugate, *BSA-594*, Fisher Scientific, Pittsburgh, PA, USA) was immobilized on two-dimensional ABS substrates. The supernatant was collected after biomolecular functionalization for each of 4 experimental

Author Manuscript Author Manuscript Author Manuscript Author Manuscript

groups (n = 3 per group): negative control (no BSA-594, plasma cleaning, or carbodiimide crosslinker); BSA-594 added with carbodiimide crosslinker without plasma cleaning; BSA-594 added after plasma cleaning but without the carbodiimide crosslinker; BSA-594 added with carbodiimide crosslinker after plasma cleaning. The amount of unattached BSA-594 remaining in the supernatant was quantified against a known standard via a fluorescence spectrophotometer (infinite M200 Pro, Tecan, Switzerland). Immobilized BSA-594 was calculated from the total BSA-594 added and the amount remaining in solution. Additionally, ABS fibers (1 mm diameter) conjugated with BSA-594 were imaged with a fluorescent microscope (Leica DMI 4000B; excitation: 596; emission: 615) using an HCImage camera (exposure time: 0.1 s) to assess the distribution of BSA-594 on the fiber surface (versus unconjugated ABS).

2.7. Cylindrical ABS–CG scaffolds to evaluate cell metabolic health

While large (7.6 cm × 2 cm × 5 mm) rectilinear constructs were used to demonstrate the efficacy of ABS-fiber reinforcement on the tensile properties of CG scaffolds, such large specimens were impractical for assays to evaluate the metabolic health of cells within the CG–ABS composites. In this case, 90,000 cells per construct would be required to match typical seeding densities of cells within CG scaffolds [51]. As a result, a second set of CG–ABS composites were generated to evaluate the impact of ABS-fiber incorporation on cell bioactivity. Here, a 10 mm diameter scaffold disk (6 mm thick) commonly-used by our laboratory for evaluating the effect of scaffold properties on cell bioactivity [41] was used. Cylindrical ABS fiber cages (10 mm dia.; 6 mm thick) were fabricated from two parallel ABS fiber rings connected by 8 parallel ABS fibers (all fibers 1 mm dia.) were incorporated into cylindrical CG scaffold disks via identical lyophilization steps as described in section 2.3. Importantly both the rectilinear (used for mechanical tests) and cylindrical (cell bioactivity) composites were designed such that the fiber volume remained relatively constant (cylindrical: 28%; rectilinear: 31%). Cylindrical CG–ABS composites were hydrated in ethanol followed by phosphate-buffered saline (PBS) then were crosslinked using carbodiimide chemistry for 1 h in a solution EDC and NHS at a molar ratio of 5:2:1 EDC:NHS:COOH where COOH represents the amount of collagen in the scaffold [7,40]. After crosslinking, cylindrical CG–ABS composites were rinsed and stored in PBS until further use.

2.8. Culture of porcine adipose tissue derived stem cells (pASCs)

Porcine adipose tissue derived stem cells (pASCs) were provided as a gift from Dr. Matthew Wheeler (U. Illinois at Urbana-Champaign) [52]. pASCs were expanded in standard tissue culture plastic in complete ASC growth medium (10% fetal bovine serum, 1% antibiotic–antimycotic in Dulbecco's Modified Eagle Medium) at 37 °C and 5% CO_2, fed every 3 days, and used at passage 7. For experiments evaluating the bioactivity of pASCs within CG–ABS composites (with or without immobilized PDGF), 9×10^4 pASCs in 20 μL microliters of growth medium were seeded onto cylindrical (height: 6 mm; radius: 5 mm) scaffold specimens containing cylindrical fiber arrays using a previously described static seeding method [5]. After 30 min to allow initial cell attachment [4,24], ABS–CG composites were transferred to complete ASC growth medium and then maintained for up to 7 days in a cell culture incubator (37 °C and 5% CO_2).

Author Manuscript Author Manuscript Author Manuscript Author Manuscript

As a two-dimensional control, well plate inserts consisting of bare or PDGF-functionalized ABS disks (0.42 cm radius; height: 0.5 cm; 10% infill, 2 shells, 200 μm layers; polystyrene extruder: 250 °C; ABS extruder: 230 °C; build plate: 110 °C; extruder speed: 90 mm/s) were generated via 3D printing. The inserts were placed into standard 24-well plates (Fisher Scientific,), seeded with porcine adipose derived stem cells (50,000 cells/well insert), and maintained for up to 7 days in a cell culture incubator (37 °C and 5% CO_2).

The mitochondrial metabolic activity of ASCs seeded in CG–ABS composites and on 2D ABS well plate inserts were quantified at day 1, 4 and 7 via alamarBlue® (Invitrogen, Carlsbad, CA). Viable, healthy cells reduce resazurin in alamarBlue solution to resorufin, which produces fluorescence. CG–ABS composites and 2D ABS well plate inserts were incubated in alamarBlue solution with gentle shaking for 1 h, and fluorescence was then measured (excitation 540 nm, emission 580 nm) on a fluorescent spectrophotometer (Tecan, Switzerland). Results were compared to a prepared standard to compute equivalent cell number. Results ($n = 5$) were reported as the relative metabolic activity compared to the number of originally seeded cells [53]. The total number of pASCs attached to the CG–ABS fiber reinforced scaffold was also quantified at day 7 using Hoechst 33258 dye (Invitrogen, Carlsbad, CA) which fluorescently labels double-stranded DNA. Briefly, scaffolds were rinsed in PBS to remove unattached and/or dead cells, then placed in a papain solution at 60 °C overnight to digest the scaffold and lyse the cells. Total cell number was determined at day 7 using a fluorescence spectrophotometer (Tecan, Switzerland). Results ($n = 5$) were compared to a prepared standard to compute cell number and were reported as the relative fold change as compared to the number of originally seeded cells [54].

2.9. Statistics

Significance was set at $p < 0.05$ and error is reported as standard error of the mean unless otherwise noted. The Levene test for equal variance was performed on all data sets to confirm validity of further statistical testing; If the Levene test showed unequal variance, the data was transformed by taking either the square root (toughness) or natural log (elastic modulus, 3D metabolic activity) and further statistical analysis was performed on the transformed data. One-way ANOVA was performed on mechanical (elastic modulus, peak stress, strain at peak stress, toughness), cell viability (alamarBlue), and proliferation (Hoescht) data followed by Tukey post-hoc tests. Mechanical tensile tests were performed with $n = 6$ samples per group, biomolecular functionalization experiments were performed with $n = 3$ samples per group, and all cell experiments were performed with $n = 5$ samples per group.

3. Results

3.1. Incorporation of ABS fibers within the CG scaffold

Following lyophilization, the CG scaffold fully incorporated the ABS fiber array (Fig. 1B). SEM analysis of transverse sections taken from the CG–ABS fiber array composite showed that the CG scaffold was directly opposed to the surface of the ABS fibers (Fig. 1C). Incorporation of the ABS fiber array was observed to add significant mechanical advantage relative to the scaffold alone; when strained to 20% strain, far in excess of the loading range

Author Manuscript Author Manuscript Author Manuscript Author Manuscript

of tissue engineering constructs for tendon applications (5% strain) [55] and the typical failure strain of the CG scaffold (15%), the ABS fiber array – and hence the CG–ABS composite – remained competent.

3.2. The mechanical properties of the CG–ABS fiber array composites can be tuned via the fiber array design

The elastic modulus, peak stress, strain at peak stress, and toughness were calculated for a series of CG–ABS composites containing increasing degrees of mechanical reinforcement (*scaffold alone; 2 mm sinusoidal fiber array; 1 mm sinusoidal fiber array; straight fiber array*; Fig. 2). The elastic modulus of the composites increased significantly ($p < 0.001$) with mechanical reinforcement, with the *straight fiber array* having the highest elastic modulus (15.05 ± 1.73 MPa), followed by *1 mm sinusoidal fiber array* (8.01 ± 0.51 MPa), *2 mm sinusoidal fiber array* (2.47 ± 0.32 MPa), and *scaffold alone* (0.22 ± 0.01 MPa). The peak stress also increased significantly ($p < 0.01$) following the same trend (*straight fiber array*: 0.91 ± 0.063 MPa; *1 mm sinusoidal fiber array*: 0.65 ± 0.075 MPa; *2 mm sinusoidal fiber array*: 0.30 ± 0.015 MPa; *scaffold alone*: 0.03 ± 0.001 MPa). The strain at peak stress was significantly ($p < 0.05$) higher for the *2 mm sinusoidal fiber array* (0.24 ± 0.03 mm/mm), though otherwise there was no significant differences between the strain at peak stress for any other groups (0.10–0.15 mm/mm). However, fiber reinforcement did significantly ($p < 0.01$) affect the overall toughness of the composites, with *straight fiber array* displaying highest toughness (151.9 ± 15.4 kJ/m^2), followed by the *2 mm sinusoidal fiber array* (77.29 ± 6.3 kJ/m^2), *1 mm sinusoidal fiber array* (75.4 ± 12.6 kJ/m^2), and *scaffold alone* (2.77 ± 0.11 kJ/m^2) (Fig. 3). Overall, ABS-fiber reinforcement increased scaffold elastic modulus by up to 68-fold, peak stress by 30-fold, and toughness by 55-fold. Results for the CG–ABS fiber composites were compared to arrays of ABS fibers alone; no significant differences were observed between the elastic modulus of the composites versus the ABS fibers alone (Supplemental Fig. 2), suggesting that processing steps for integrating the ABS fibers within the CG scaffold do not affect the mechanical stability of the fiber array itself.

3.3. Selective attachment of a model protein to the ABS fiber arrays via carbodiimide chemistry

Using fluorescently labeled BSA (BSA-594) as a model protein we confirmed that exposing plasma treated ABS to a protein of interest in the presence of EDC:NHS chemistry led to efficient covalent immobilization of the protein on the ABS fiber (Fig. 4). No appreciable immobilization was observed when the BSA was simply exposed to the fiber or when either the plasma treatment or the EDC:NHS crosslinker were removed. However, significantly higher BSA attachment was observed when both plasma treatment and EDC:NHS crosslinking were employed, with PSA immobilization assessed via quantitative metrics (Fig. 4A) or fluorescent image analysis (Fig. 4B).

3.4. Metabolic activity of pASCs on ABS substrates as a function of immobilized PDGF

The metabolic activity of pASCs was measured at days 1, 4 and 7 on 2D ABS well plate inserts. Although metabolic activity increased at day 4 versus initial seeding conditions regardless of PDGF availability, it dropped to approximately initial seeding conditions by day 7. However, ABS substrates functionalized with PDGF promoted a significant increase

Author Manuscript Author Manuscript Author Manuscript Author Manuscript

in pASC metabolic activity compared to pASCs on ABS alone group at every time point ($p < 0.05$). (Fig. 5A, B).

3.5. The bioactivity of pASCs within CG scaffold-ABS fiber composites

The metabolic activity of pASCs maintained within the CG–ABS fiber array composites increased significantly in all groups with time (from day 1 to day 7; $p < 0.05$). While not significant ($p = 0.11$) the metabolic activity of pASCs in CG–ABS fiber array composites containing covalently attached PDGF was higher compared to composites containing bare ABS fibers (Fig. 5C). However, by day 7 there was a significant increase in the total number of pASCs within composites containing PDGF-functionalized ABS fiber arrays ($p < 0.05$) (Fig. 5D).

4. Discussion

Herein, we report an adaptable approach to mechanically reinforce a CG scaffold under development for tendon repair applications via incorporation of arrays of polymeric fibers created via three-dimensional printing methods. This approach led to significant (30- to 68-fold) increases in the overall mechanical performance of the CG composite in a manner that did not affect the metabolic health of cells within the matrix but which provides significant flexibility for tailoring overall construct mechanical properties. Additionally, we demonstrated the ability to functionalize the reinforcing fibers with activity-inducing biomolecules to further instruct cell response. Together, this approach offers a new avenue for designing high-porosity biomaterials for high-strength applications.

Increasingly, tissue engineering requires biomaterials with sufficient strength to match the mechanical properties of a healthy tissue while leaving the material porous enough and with high enough specific surface area to support cellular penetration, attachment, and sufficient nutrient biotransport. Composite designs offer a potential solution to this trade-off between sufficient porosity and high mechanical strength. Previous work in our lab has demonstrates a core–shell composite design inspired by porcupine quills and plant stems [44,45]. Here, a highly porous CG scaffold *core* was surrounded by a high density collagen membrane *shell* capable of increasing the composite modulus by over 30-fold [13]. To increase nutrient transport and cell penetration, periodic perforation could be added to the shell, but at the expense of strength [46]. While a useful demonstration of composite design, these constructs were difficult to adapt for the unique geometric needs of patient-specific defects. Work by Mauck et al. has explored the idea of using sacrificial chemistries for electrospun fibers to create fibrous mats for tissue engineering applications with enhanced permeability and cell infiltration [56]. However, these constructs are limited to relatively thin two-dimensional geometries and as such are difficult to individualize for personalized tissue engineering applications which require a unique, specifically shaped 3D biomaterial for patient-specific injuries.

The rapid growth of commercial 3D printing tools offers new potential to personalize biomaterials for tissue engineering applications. Advances in nozzle and ink design have allowed extrusion and printing of some cell containing hydrogels, yet the resolution of many commercial 3D printing tools is limited to millimeter-scale features [57]. However, the

Author Manuscript Author Manuscript Author Manuscript Author Manuscript

ability to generate customizable reinforcement structures to be integrated into more traditional tissue engineering biomaterials have been explored in only a limited manner [58]. The goal of this work therefore was to integrate the high strength, yet low spatial resolution of 3D printing techniques with a biomaterial with micrometer-scale features to create a composite with the best attributes of both, and was inspired by the longitudinal fibers found as reinforcing structures in plant stems [59]. Our novel CG–ABS composites described here are an example of multi-functional biomaterials, using the ABS fiber array to selectively modify both mechanical strength and the incorporation of a biomolecule of interest independent of the CG scaffold design. Native tendon *in vivo* typically experiences strain profiles ranging from relatively small for position tendons (max. strain: 3.1%) [60] to significantly larger for energy storing tendons (e.g., Achilles tendon; max strain: 10.3%) [61], with a peak stresses of approximately 15–30 MPa, as well as a range of elastic moduli (0.45 GPa to 1.2 GPa) [35,62,63]. Although our composites fall short of matching these mechanical properties (especially at maximum loads which are typically avoided after injury) they are mechanically competent within the physiologically relevant range of strain, and have drastically improved properties compared to the collagen scaffold alone. As the composite is meant to be a regenerative template which provides a microenvironment to enable cell recruitment, proliferation, and matrix deposition, our focus here is to validate the fiber-reinforced biomimetic scaffold design paradigm. These composites show significantly improved and tunable mechanical properties compared to CG scaffolds alone, improved bioactivity when compared to ABS constructs alone, and lose neither mechanical integrity nor bioactivity when combined.

A critical need in the design of biomaterials for increasingly complex musculoskeletal applications is the ability to orthogonally tune mechanics and bioactivity over a desired functional range. These needs may extend across many scales. The stress a biomaterial scaffold may experience *in vivo* often exceeds the amount of stress the scaffold alone can withstand before failure. Our work demonstrates an approach to design a composite with a heightened modulus to result in desired levels of strain when exposed to a physiologically relevant load (or stress). Incorporating the ABS fiber arrays within a collagen composite allows the cells to experience a defined amount of strain, while withstanding an increased amount of stress. This approach also suggests the capability to tune the elastic modulus, toughness, and peak stress/strain to meet patient-specific criteria. Ongoing efforts are exploring selective modification of the total number of ABS fibers, the thickness of the fibers, and the longitudinal changes in fiber architecture (*e.g.*, sinusoidal amplitude, period) along the fibers in order to regionally manipulate the local stress–strain fields during loading. Ongoing efforts are also exploring ASC-response to extended mechanical stimulation (constant strain vs. constant stress conditions) within this series of fiber-reinforced constructs, with results expected to add significantly to our understanding of how mechanical reinforcement at the construct scale alters ASC differentiation profiles at the micro-scale.

ABS was chosen as a model system for its ease of printing via commercially available 3D printing tools, its strength, and the potential for surface modification to facilitate covalent immobilization of biomolecules. However, long-term development of fiber-reinforced composites will likely require a different polymer that would support a wider range of

Author Manuscript Author Manuscript Author Manuscript Author Manuscript

functionality (*e.g.*, cell-adhesion, growth factor release, degradability). Given the low specific surface area of the ABS within the CG–ABS composite, cells likely primarily interact with the CG scaffold in the full composite. However, examining the role of PDGF-immobilization on 2D ABS substrates (Fig. 5), pASCs were forced to interact directly with the ABS. While pASC metabolic activity was higher at all timepoints on ABS substrates containing surface immobilized PDGF versus ABS alone, an observation consistent with previous efforts in our group showing the efficacy of covalently-tethered PDGF [26], ABS itself did not support pASC expansion. Translated to the ABS-fiber reinforced CG composite, pASC metabolism increased significantly ($p < 0.05$) over the 7 day culture period and total cell expansion was significantly higher ($p < 0.05$) for CG–ABS composites containing covalently-immobilized PDGF (Fig. 5C, D). This suggests construct mechanical behavior can be defined by the ABS fiber arrays, while cell response is likely dominated by the porous CG scaffold material. Given the surface area of ABS within the current composite design, effective use of the ABS fibers to present activity-inducing growth factors while maximizing cellular activity within the collagen scaffold composite will require new methodological development. As there is a tradeoff between mechanics and bioactivity, even in our composite constructs, ongoing efforts are looking to solve a new optimization problem: minimizing the volume fraction of the ABS fibers while maximizing the enhancement in mechanics seen for the composite as a whole. To this end we are exploring more complex fiber designs, both increasing the number of ABS fibers as well as exploring the use of enzymatically cleavable linkers to provide temporal control over the bioavailability of immobilized biomolecules.

5. Conclusions

The need to balance biomechanical and bioactivity requirements in the design of tissue engineering biomaterials for musculoskeletal applications requires a new design toolbox. While typically incapable of generating biomaterials with micrometer-scale features, three-dimensional printing offers a unique way to generate composite biomaterials. Herein we demonstrates a composite design that integrates arrays of ABS fibers with tailorable mechanical properties generated via 3D printing into a collagen-GAG scaffold with high bioactivity under development for tendon repair applications. In addition to mechanical reinforcement, we also show that the fiber array offers a platform to integrate activity-inducing doses of growth factors into the construct in a manner orthogonal to the design of the collagen scaffold itself. The paradigm described here represents a novel departure from current methods to address bioactivity-biomechanical trade-offs in biomaterial design. This approach also offers the potential to integrate patient-customizable reinforcement elements into a standardized scaffold as well as the ability to locally tune the permissible stress–strain behavior of the composite in order to meet the needs of a variety of musculoskeletal tissues including insertional zones between disparate tissues such as tendon and bone.

Supplementary Material

Refer to Web version on PubMed Central for supplementary material.

Author Manuscript Author Manuscript Author Manuscript Author Manuscript

Acknowledgments

The authors would like to acknowledge Dr. Hyun Joon Kong (UIUC) for access to mechanical testing facilities, Dr. Sandra McMasters (SCS, UIUC) for preparation of culture media, Dr. Matthew Wheeler for providing pASCs, and Richard Graybill for assistance with oxygen plasma treatment. Research reported in this publication was supported by the National Institute of Arthritis and Musculoskeletal and Skin Diseases of the National Institutes of Health under Award Numbers R21 AR063331. LCM was partially funded via National Science Foundation Grant 0965918 *IGERT: Training the Next Generation of Researchers in Cellular & Molecular Mechanics and BioNanotechnology*, as well as the Support for Under-Represented Groups in Engineering (SURGE) Fellowship and the DuPont Science and Engineering Fellowship. This research was carried out in part in the Frederick Seitz Materials Research Laboratory Central Facilities, University of Illinois, which are partially supported by the U.S. Department of Energy under Grants DE-FG02-07ER46453 and DE-FG02-07ER46471.

References

1. James R, Kesturu G, Balian G, Chhabra AB. Tendon: biology, biomechanics, repair, growth factors, and evolving treatment options. J. Hand Surg. Am. 2008; 33:102–112. [PubMed: 18261674]
2. Xu Y, Murrell GA. The basic science of tendinopathy. Clin. Orthop. Related Res. 2008; 466:1528–1538.
3. Liu Y, Ramanath HS, Wang DA. Tendon tissue engineering using scaffold enhancing strategies. Trends Biotechnol. 2008; 26:201–209. [PubMed: 18295915]
4. O'Brien FJ, Harley BA, Yannas IV, Gibson LJ. The effect of pore size on cell adhesion in collagen-GAG scaffolds. Biomaterials. 2005; 26:433–441. [PubMed: 15275817]
5. O'Brien FJ, Harley BA, Waller MA, Yannas IV, Gibson LJ, Prendergast PJ. The effect of pore size on permeability and cell attachment in collagen scaffolds for tissue engineering. Technol. Health Care. 2007; 15:3–17. [PubMed: 17264409]
6. Harley BA, Freyman TM, Wong MQ, Gibson LJ. A new technique for calculating individual dermal fibroblast contractile forces generated within collagen-gag scaffolds. Biophys. J. 2007; 93:2911–2922. [PubMed: 17586570]
7. Olde Damink LHH, Dijkstra PJ, Van Luyn MJA, Van Wachem PB, Nieuwenhuis P, Feijen J. Cross-linking of dermal sheep collagen using a water-soluble carbodiimide. Biomaterials. 1996; 17:765–773. [PubMed: 8730960]
8. Chamberlain LJ, Yannas IV, Hsu H-P, Strichartz G, Spector M. Collagen-GAG substrate enhances the quality of nerve regeneration through collagen tubes up to level of autograft. Exp. Neurol. 1998; 154:315–329. [PubMed: 9878170]
9. Freyman TM, Yannas IV, Pek YS, Yokoo R, Gibson LJ. Micromechanics of fibroblast contraction of a collagen-GAG matrix. Exp. Cell Res. 2001; 269:140–153. [PubMed: 11525647]
10. Harley BA, Kim HD, Zaman MH, Yannas IV, Lauffenburger DA, Gibson LJ. Microarchitecture of three-dimensional scaffolds influences cell migration behavior via junction interactions. Biophys. J. 2008; 95:4013–4024. [PubMed: 18621811]
11. Mathew AP, Oksman K, Pierron D, Harmand M-F. Biocompatible fibrous networks of cellulose nanofibres and collagen crosslinked using genipin: potential as artificial ligament/tendons. Macromolecular Bioscience. 2012 n/a-n/a.
12. Galatz LM, Sandell LJ, Rothermich SY, Das R, Mastny A, Havlioglu N, Silva MJ, Thomopoulos S. Characteristics of the rat supraspinatus tendon during tendon-to-bone healing after acute injury. J. Orthop. Res. 2006; 24:541–550. [PubMed: 16456829]
13. Caliari SR, Ramirez MA, Harley BAC. The development of collagen-GAG scaffold-membrane composites for tendon tissue engineering. Biomaterials. 2011; 32:8990–8998. [PubMed: 21880362]
14. Levingstone TJ, Matsiko A, Dickson GR, O'Brien FJ, Gleeson JP. A biomimetic multi-layered collagen-based scaffold for osteochondral repair. Acta Biomater. 2014; 10:1996–2004. [PubMed: 24418437]
15. Kanungo BP, Silva E, Vliet KV, Gibson LJ. Characterization of mineralized collagen–glycosaminoglycan scaffolds for bone regeneration. Acta Biomater. 2008; 4:490–503. [PubMed: 18294943]

Author Manuscript Author Manuscript Author Manuscript Author Manuscript

16. Ferreira AM, Gentile P, Chiono V, Ciardelli G. Collagen for bone tissue regeneration. Acta Biomater. 2012; 8:3191–3200. [PubMed: 22705634]
17. Capito RM, Spector M. Collagen scaffolds for nonviral IGF-1 gene delivery in articular cartilage tissue engineering. Gene therapy. 2007; 14:721–732. [PubMed: 17315042]
18. Harley BA, Lynn AK, Wissner-Gross Z, Bonfield W, Yannas IV, Gibson LJ. Design of a multiphase osteochondral scaffold. II. Fabrication of a mineralized collagen-glycosaminoglycan scaffold. J. Biomed. Mater. Res. Part A. 2010; 92A:1066–1077.
19. Caliari SR, Grier WK, Weisgerber DW, Mahmassani Z, Boppart MD, Harley BAC. Collagen scaffolds incorporating coincident gradations of instructive structural and biochemical cues for osteotendinous junction engineering. Adv. Healthcare Mater. 2015; 4:831–837.
20. Harley BA, Lynn AK, Wissner-Gross Z, Bonfield W, Yannas IV, Gibson LJ. Design of a multiphase osteochondral scaffold III: fabrication of layered scaffolds with continuous interfaces. J. Biomed. Mater. Res. A. 2010; 92:1078–1093. [PubMed: 19301263]
21. Quinlan E, Partap S, Azevedo MM, Jell G, Stevens MM, O'Brien FJ. Hypoxia-mimicking bioactive glass/collagen glycosaminoglycan composite scaffolds to enhance angiogenesis and bone repair. Biomaterials. 2015; 52:358–366. [PubMed: 25818442]
22. Lyons FG, Gleeson JP, Partap S, Coghlan K, O'Brien FJ. Novel microhydroxyapatite particles in a collagen scaffold: a bioactive bone void filler? Clin Orthop. Related Res. 2014; 472:1318–1328.
23. Weisgerber DW, Caliari SR, Harley BAC. Mineralized collagen scaffolds induce hMSC osteogenesis and matrix remodeling. Biomater. Sci. 2015; 3:533–542. [PubMed: 25937924]
24. Caliari SR, Harley BAC. The effect of anisotropic collagen-GAG scaffolds and growth factor supplementation on tendon cell recruitment, alignment, and metabolic activity. Biomaterials. 2011; 32:5330–5340. [PubMed: 21550653]
25. McCoy RJ, Widaa A, Watters KM, Wuerstle M, Stallings RL, Duffy GP, O'Brien FJ. Orchestrating osteogenic differentiation of mesenchymal stem cells— identification of placental growth factor as a mechanosensitive gene with a pro-osteogenic role. Stem Cells. 2013; 31:2420–2431. [PubMed: 23897668]
26. Caliari SR, Harley BA. Composite growth factor supplementation strategies to enhance tenocyte bioactivity in aligned collagen-GAG scaffolds. Tissue Eng. Part A. 2013; 19:1100–1112. [PubMed: 23157454]
27. Mullen LM, Best SM, Ghose S, Wardale J, Rushton N, Cameron RE. Bioactive IGF-1 release from collagen-GAG scaffold to enhance cartilage repair in vitro. J. Mater. Sci. Mater. Med. 2015; 26:5325. [PubMed: 25577208]
28. Miyagi Y, Chiu LL, Cimini M, Weisel RD, Radisic M, Li RK. Biodegradable collagen patch with covalently immobilized VEGF for myocardial repair. Biomaterials. 2011; 32:1280–1290. [PubMed: 21035179]
29. Martin TA, Caliari SR, Williford PD, Harley BA, Bailey RC. The generation of biomolecular patterns in highly porous collagen-GAG scaffolds using direct photolithography. Biomaterials. 2011; 32:3949–3957. [PubMed: 21397322]
30. Alsop AT, Pence JC, Weisgerber DW, Harley BAC, Bailey RC. Photopatterning of VEGF within collagen-GAG scaffolds can induce a spatially confined response in human umbilical vein endothelial cells. Acta Biomater. 2014; 10:4715–4722. [PubMed: 25016280]
31. Banks JM, Mozdzen LC, Harley BAC, Bailey RC. The combined effects of matrix stiffness and growth factor immobilization on the bioactivity and differentiation capabilities of adipose-derived stem cells. Biomaterials. 2014; 35:8951–8959. [PubMed: 25085859]
32. Hortensius RA, Becraft JR, Pack DW, Harley BAC. The effect of glycosaminoglycan content on polyethylenimine-based gene delivery within three-dimensional collagen-GAG scaffolds. Biomater. Sci. 2015; 3:645–654. [PubMed: 26097698]
33. Hortensius RA, Harley BA. The use of bioinspired alterations in the glycosaminoglycan content of collagen-GAG scaffolds to regulate cell activity. Biomaterials. 2013; 34:7645–7652. [PubMed: 23871542]
34. Thorpe CT, Stark RJ, Goodship AE, Birch HL. Mechanical properties of the equine superficial digital flexor tendon relate to specific collagen cross-link levels. Equine Vet. J. 2010; 42(Suppl 38):538–543.

Author Manuscript Author Manuscript Author Manuscript Author Manuscript

35. Thorpe CT, Udeze CP, Birch HL, Clegg PD, Screen HRC. Specialization of tendon mechanical properties results from interfascicular differences. J. R. Soc. Interface. 2012; 9:3108–3117. [PubMed: 22764132]
36. Moore TLA, Gibson LJ. Modeling modulus reduction in bovine trabecular bone damaged in compression. J. Biomech. Eng.-Trans. ASME. 2001; 123:613–622.
37. Michel MC, Guo XDE, Gibson LJ, Mcmahon TA, Hayes WC. Compressive fatigue behavior of bovine trabecular bone. J. Biomech. 1993; 26:453–463. [PubMed: 8478349]
38. Wopenka B, Kent A, Pasteris JD, Yoon Y, Thomopoulos S. The tendon-to-bone transition of the rotator cuff: a preliminary Raman spectroscopic study documenting the gradual mineralization across the insertion in rat tissue samples. Appl. Spectrosc. 2008; 62:1285–1294. [PubMed: 19094386]
39. Murphy CM, Haugh MG, O'Brien FJ. The effect of mean pore size on cell attachment, proliferation and migration in collagen-glycosaminoglycan scaffolds for bone tissue engineering. Biomaterials. 2010; 31:461–466. [PubMed: 19819008]
40. Harley B, Leung J, Silva E, Gibson L. Mechanical characterization of collagen–glycosaminoglycan scaffolds. Acta Biomater. 2007; 3:463–474. [PubMed: 17349829]
41. Weisgerber DW, Kelkhoff DO, Caliari SR, Harley BAC. The impact of discrete compartments of a multi-compartment collagen-GAG scaffold on overall construct biophysical properties. J. Mech. Behav. Biomed. Mater. 2013; 28:26–36. [PubMed: 23973610]
42. Gibson, LJ.; Ashby, MF.; Harley, BA. Cellular Materials in Nature and Medicine. Cambridge, U.K.: Cambridge University Press; 2010.
43. Keays SL, Bullock-Saxton JE, Keays AC, Newcombe PA, Bullock MI. A 6-year follow-up of the effect of graft site on strength, stability, range of motion, function, and joint degeneration after anterior cruciate ligament reconstruction patellar tendon versus semitendinosus and gracilis tendon graft. Am. J. Sports Med. 2007; 35:729–739. [PubMed: 17322130]
44. Gibson LJ, Ashby MF, Karam GN, Wegst U, Shercliff HR. The mechanical-properties of natural materials 2. Microstructures for mechanical efficiency. Philos. Trans. R. Soc. London A. 1995; 450:141–162.
45. Karam GN, Gibson LJ. Biomimicking of animal quills and plant stems - natural cylindrical-shells with foam cores. Mater. Sci. Eng. C Biomimetics Mater. Sens Syst. 1994; 2:113–132.
46. Caliari SR, Mozdzen LC, Armitage O, Oyen ML, Harley BAC. Award winner in the young investigator category, 2014 Society for biomaterials annual meeting and exposition, denver, colorado, april 16–19, 2014: periodically perforated core–shell collagen biomaterials balance cell infiltration, bioactivity, and mechanical properties. J. Biomed. Res. A. 2014; 102:917–927.
47. Yannas IV, Lee E, Orgill DP, Skrabut EM, Murphy GF. Synthesis and characterization of a model extracellular matrix that induces partial regeneration of adult mammalian skin. Proc. Nat. Acad. Sci. 1989; 86:933–937. [PubMed: 2915988]
48. O'Brien FJ, Harley BA, Yannas IV, Gibson L. Influence of freezing rate on pore structure in freeze-dried collagen-GAG scaffolds. Biomaterials. 2004; 25:1077–1086. [PubMed: 14615173]
49. Harley BA, Leung JH, Silva EC, Gibson LJ. Mechanical characterization of collagen-glycosaminoglycan scaffolds. Acta Biomater. 2007; 3:463–474. [PubMed: 17349829]
50. Ma Z, He W, Yong T, Ramakrishna S. Grafting of gelatin on electrospun poly (caprolactone) nanofibers to improve endothelial cell spreading and proliferation and to control cell orientation. Tissue Eng. 2005; 11:1149–1158. [PubMed: 16144451]
51. Caliari SR, Weisgerber DW, Ramirez MA, Kelkhoff DO, Harley BAC. The influence of collagen-glycosaminoglycan scaffold relative density and microstructural anisotropy on tenocyte bioactivity and transcriptomic stability. J. Mech. Behav. Biomed. Mater. 2012; 11:27–40. [PubMed: 22658152]
52. Monaco E, Lima A, Bionaz M, Maki A, Wilson S, Hurley WL, Wheeler MB. Morphological and transcriptomic comparison of adipose and bone marrow derived porcine stem cells. Open Tissue Eng. Regen. Med. J. 2009:20–33.
53. Tierney CM, Jaasma MJ, O'Brien FJ. Osteoblast activity on collagen-GAG scaffolds is affected by collagen and GAG concentrations. J. Biomed. Mater. Res. A. 2009; 91A:92–101. [PubMed: 18767061]

Author Manuscript Author Manuscript Author Manuscript Author Manuscript

54. Kim YJ, Sah RLY, Doong JYH, Grodzinsky AJ. Fluorometric assay of DNA in cartilage explants using Hoechst 33258. Anal. Biochem. 1988; 174:168–176. [PubMed: 2464289]
55. Maganaris CN, Paul JP. In vivo human tendon mechanical properties. J. Physiol. 1999; 521(Pt 1): 307–313. [PubMed: 10562354]
56. Baker BM, Shah RP, Silverstein AM, Esterhai JL, Burdick JA, Mauck RL. Sacrificial nanofibrous composites provide instruction without impediment and enable functional tissue formation. Proc. Nat. Acad. Sci. U.S.A. 2012; 109:14176–14181.
57. Mironov V, Boland T, Trusk T, Forgacs G, Markwald RR. Organ printing: computer-aided jet-based 3D tissue engineering. Trends Biotechnol. 2003; 21:157–161. [PubMed: 12679063]
58. Serra T, Planell JA, Navarro M. High-resolution PLA-based composite scaffolds via 3-D printing technology. Acta Biomater. 2013; 9:5521–5530. [PubMed: 23142224]
59. Speck T, Burgert I. Plant stems: functional design and mechanics. Ann. Rev. Mater. Res. 2011; 41:169–193.
60. Maganaris CN, Paul JP. In vivo human tendinous tissue stretch upon maximum muscle force generation. J. Biomech. 2000; 33:1453–1459. [PubMed: 10940404]
61. Lichtwark GA, Wilson AM. In vivo mechanical properties of the human Achilles tendon during one-legged hopping. J. Exp. Biol. 2005; 208:4715–4725. [PubMed: 16326953]
62. Abrahams M. Mechanical behaviour of tendon In vitro. Med. Biol. Eng. 1967; 5:433–443. [PubMed: 6069823]
63. Maganaris CN, Paul JP. In vivo human tendon mechanical properties. J. Physiol. 1999; 521:307–313. [PubMed: 10562354]

Author Manuscript Author Manuscript Author Manuscript Author Manuscript

Statement of Significance

Tendon injuries account for more than 32 million injuries each year in the US alone. Current techniques use allografts to mitigate poor functional outcomes, but are not ideal platforms to induce functional regeneration following injury. Tissue engineering approaches using biomaterial substrates have significant potential for addressing these defects. However, the high porosity required to facilitate cell infiltration and nutrient transport often dictates that the resultant biomaterials has insufficient biomechanical strength. Here we describe the use of three-dimensional printing techniques to generate customizable fiber arrays from ABS polymer that can be incorporated into a collagen scaffold under development for tendon repair applications. Notably, the mechanical performance of the fiber-scaffold composite can be defined by the fiber array independent of the bioactivity of the collagen scaffold design. Further, the fiber array provides a substrate for growth factor delivery to aid healing.

Author Manuscript Author Manuscript Author Manuscript Author Manuscript

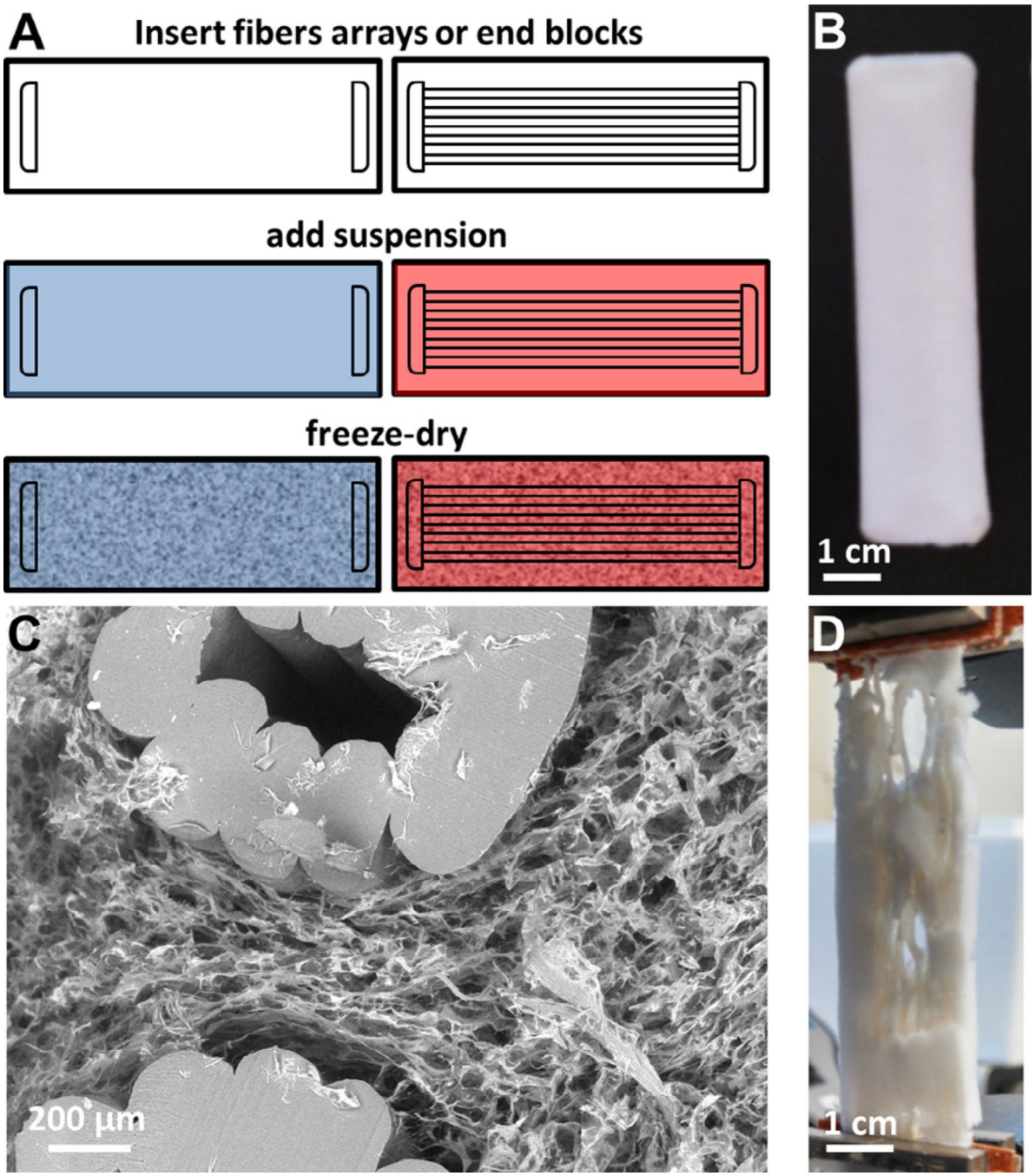

Fig. 1.

Structurally reinforced scaffold-fiber composite. (A) Schematic for creating CG scaffolds without (left) and with (right) ABS polymeric fibers embedded within. Both contain ABS polymer end blocks to facilitate mechanical testing. (B) ABS-fiber reinforced scaffold; fibers are completely incorporated within the scaffold. (C) Representative scanning electron microscopy (SEM) image of transverse section thought fiber-reinforced scaffold showing cross-section of ABS fibers and CG scaffold. Scale bar: 200 µm. (D) ABS-fiber reinforced

scaffold strained to 20% strain in tension; although the scaffold would have failed, fiber reinforcement holds the composite together well past physiological strains.

Author Manuscript Author Manuscript Author Manuscript Author Manuscript

Author Manuscript Author Manuscript Author Manuscript Author Manuscript

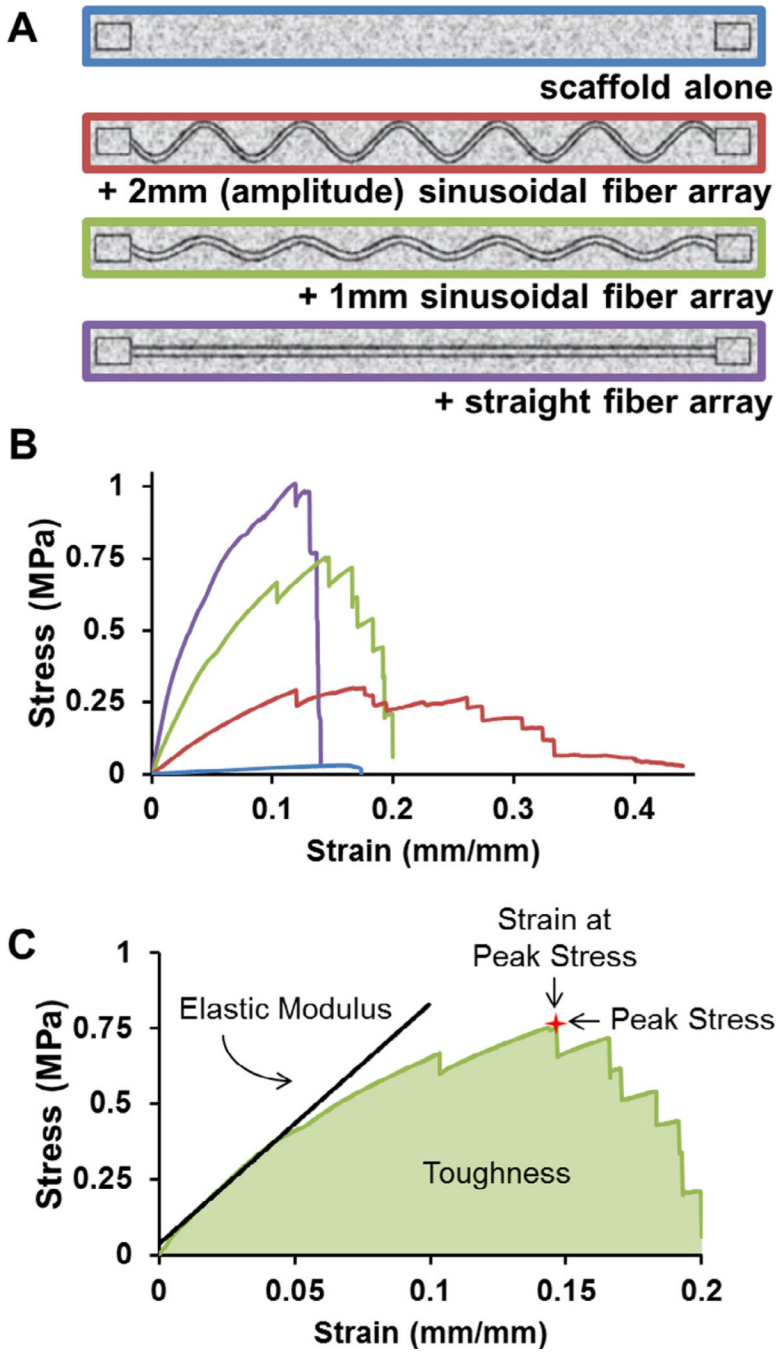

Fig. 2.

Mechanical behavior of fiber-reinforced scaffolds. (A) The tensile behavior of ABS–CG composites was assessed for four discrete: scaffold alone; 2 mm sinusoidal fiber array; 1 mm sinusoidal fiber array; straight fiber array. All fiber-reinforced variants were contained 9 parallel fibers (each 1 mm diameter) connecting ABS end blocks to facilitate clamping during tensile tests. The scaffold alone variants also contained ABS end blocks to facilitate clamping. (B) Representative stress–strain curves of all four variants. (C) Diagram depicting how the mechanical properties for each sample were measured. Elastic modulus was taken

Author Manuscript Author Manuscript Author Manuscript Author Manuscript

as the slope of the linear elastic region of the curve. Peak stress was taken as the maximum stress the sample reached, and strain at peak stress was taken as the strain (extension divided by cross-sectional area) at this same point. Finally, toughness was taken as the area under the stress–strain curve before failure.

Author Manuscript Author Manuscript Author Manuscript Author Manuscript

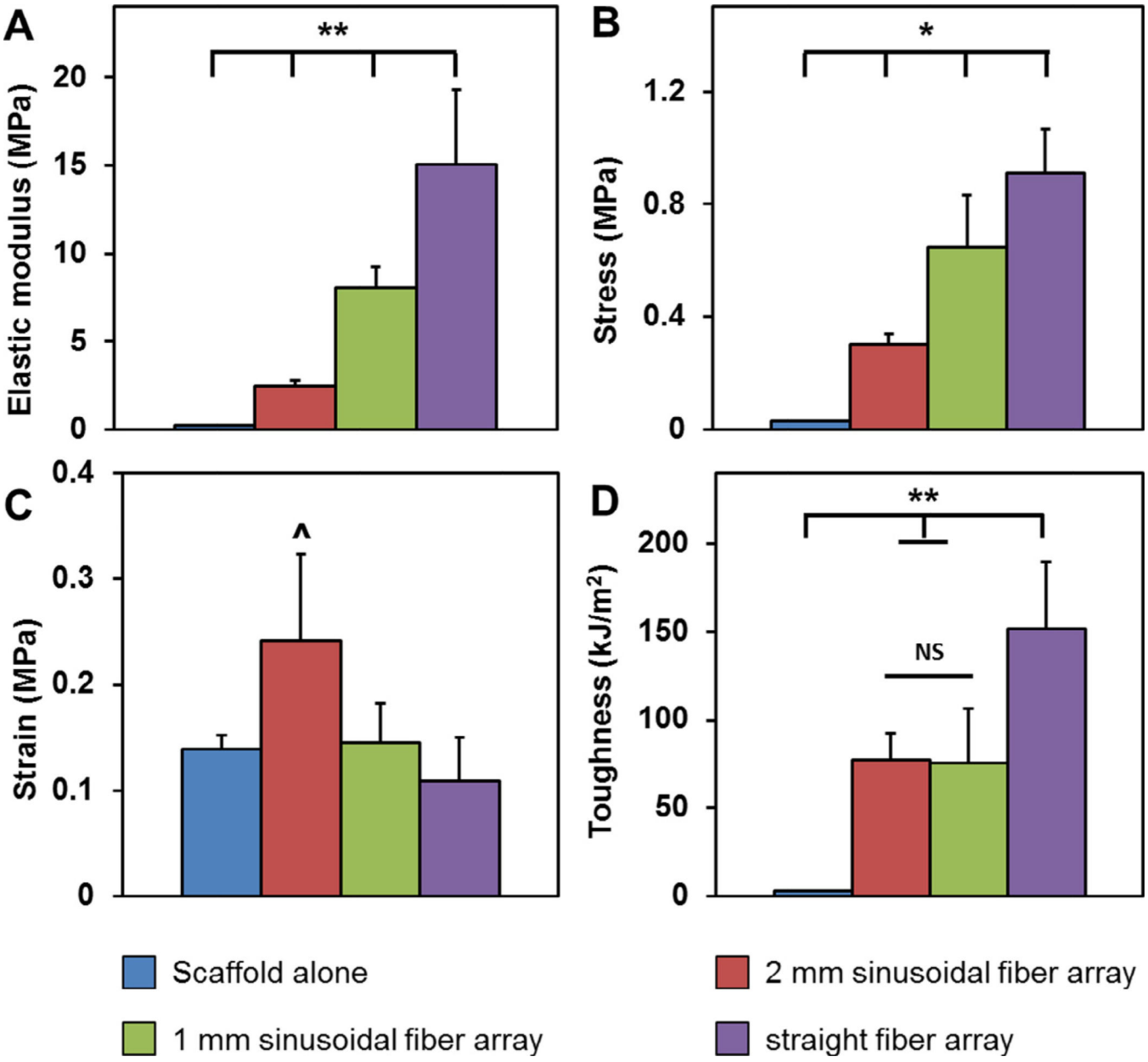

Fig. 3.

Mechanical properties of ABS-fiber reinforced CG scaffold. Elastic modulus (A) and peak stress (B) increased significantly with increasing degree of fiber reinforcement. (C) Strain at peak stress remained unchanged with the exception of the most compliant fiber-reinforcement variant. (D) The toughness of the fiber-reinforced composites was significantly greater than the scaffold alone and increased with degree of fiber reinforcement. ^: $p < 0.05$; *: $p < 0.01$; **: $p < 0.001$.

Author Manuscript Author Manuscript Author Manuscript Author Manuscript

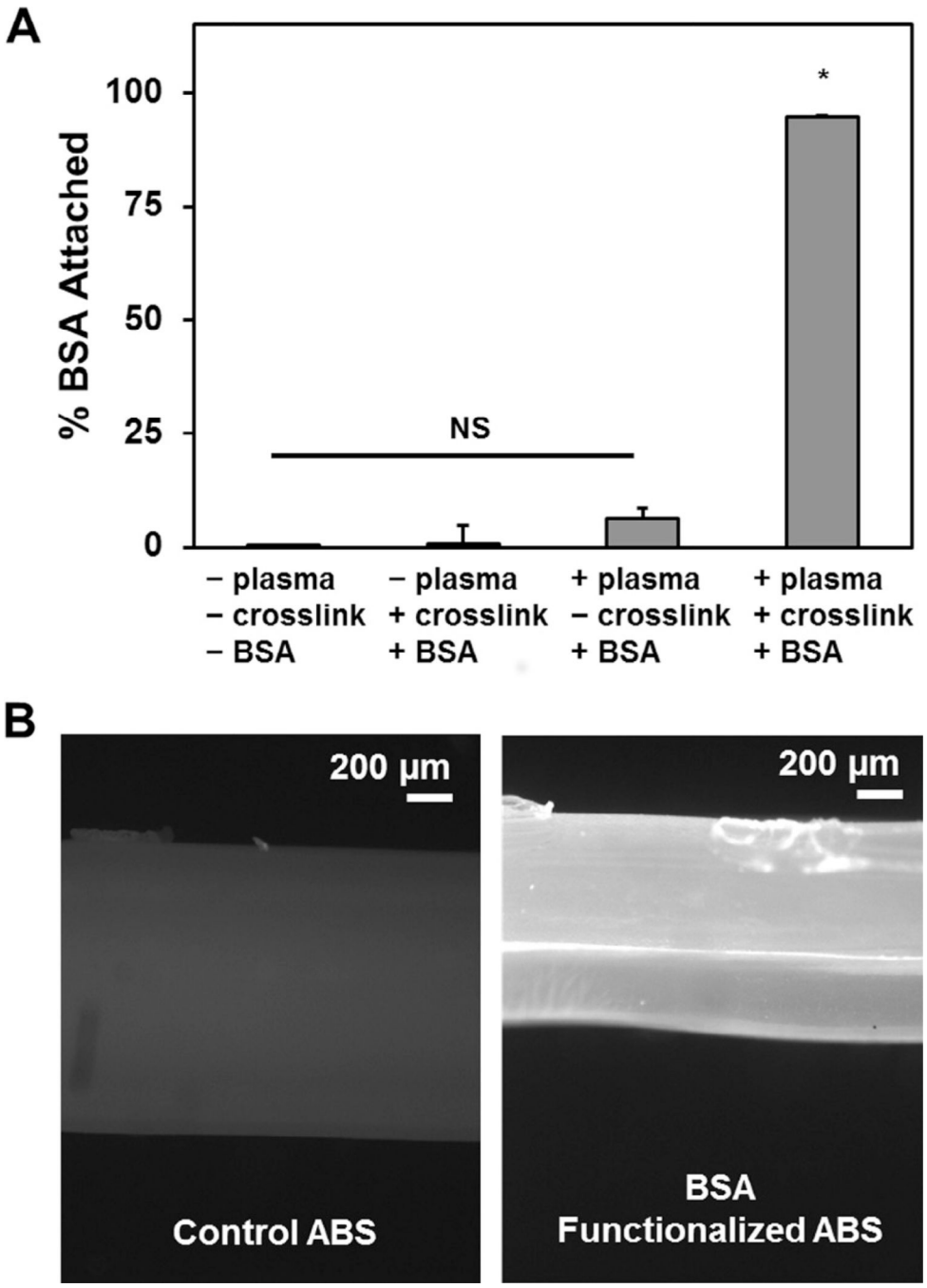

Fig. 4.

Covalent attachment of biomolecular cues via ABS-fibers. (A) Attachment of a model protein (BSA) to ABS substrates via sequential oxygen plasma treatment followed by carbodiimide crosslinking in the presence of fluorescently labeled BSA. Both plasma treatment then carbodiimide crosslinking are required to facilitate covalent biomolecule incorporation. (B) Representative fluorescent images of control ABS fibers (left) and BSA-functionalized ABS fibers (right). *: $p < 0.001$.

Author Manuscript Author Manuscript Author Manuscript Author Manuscript

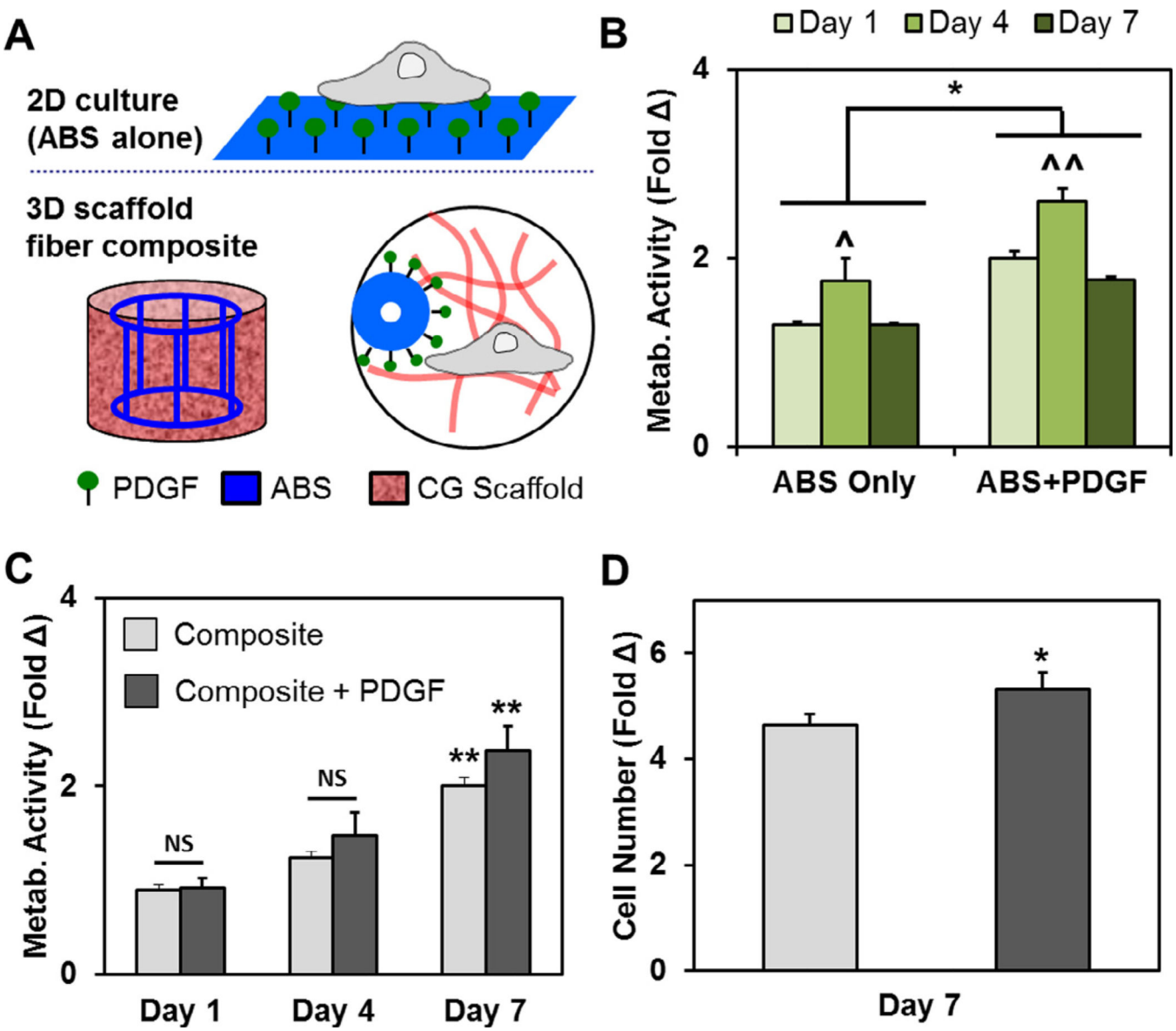

Fig. 5.

Covalent presentation of PDGF promotes changes in cell number and metabolic activity. (A) pASCs were cultured on ABS or PGDF-functionalized ABS substrates (2D); pASCs were subsequently cultured in CG scaffolds containing ABS fiber reinforcement or PDGF-functionalized ABS fiber reinforcement. (B) The metabolic activity of pASCs was higher when cultured on PDGF-decorated ABS substrates than ABS substrate controls at each time point. In both cases, the highest metabolic activity was observed at day 4. (C) The metabolic activity of pASCs significantly increased over 7 day culture in CG scaffolds containing either ABS fibers (composite) or PDGF-decorated ABS fibers (composite + PDGF). (D) Additionally, the overall cell number was significantly higher after 7 days in CG scaffolds containing PDGF-decorated fibers. *: $p < 0.05$; ^: $p < 0.01$ compared to other timepoints for

the same ABS group; ^^: $p < 0.001$ compared to other timepoints for the same ABS group; ** $p < 0.05$ compared to days 1 and 4.

Author Manuscript Author Manuscript Author Manuscript Author Manuscript